doi:10.1093/brain/awx275 BRAIN 2017: 140; 3204–3214 | 3204

BRAIN
A JOURNAL OF NEUROLOGY

Synaptic phosphorylated α-synuclein in dementia with Lewy bodies

Martí Colom-Cadena,[1,2] Jordi Pegueroles,[1,2] Abigail G. Herrmann,[3] Christopher M. Henstridge,[3] Laia Muñoz,[1,2] Marta Querol-Vilaseca,[1,2] Carla San Martín-Paniello,[1,2] Joan Luque-Cabecerans,[1,2] Jordi Clarimon,[1,2] Olivia Belbin,[1,2] Raúl Núñez-Llaves,[1,2] Rafael Blesa,[1,2] Colin Smith,[4] Chris-Anne McKenzie,[4] Matthew P. Frosch,[5] Allyson Roe,[5] Juan Fortea,[1,2] Jordi Andilla,[6] Pablo Loza-Alvarez,[6] Ellen Gelpi,[7] Bradley T. Hyman,[5] Tara L. Spires-Jones[3,*] and Alberto Lleó[1,2,*]

*These authors contributed equally to this work.

Dementia with Lewy bodies is characterized by the accumulation of Lewy bodies and Lewy neurites in the CNS, both of which are composed mainly of aggregated α-synuclein phosphorylated at Ser129. Although phosphorylated α-synuclein is believed to exert toxic effects at the synapse in dementia with Lewy bodies and other α-synucleinopathies, direct evidence for the precise synaptic localization has been difficult to achieve due to the lack of adequate optical microscopic resolution to study human synapses. In the present study we applied array tomography, a microscopy technique that combines ultrathin sectioning of tissue with immunofluorescence allowing precise identification of small structures, to quantitatively investigate the synaptic phosphorylated α-synuclein pathology in dementia with Lewy bodies. We performed array tomography on human brain samples from five patients with dementia with Lewy bodies, five patients with Alzheimer's disease and five healthy control subjects to analyse the presence of phosphorylated α-synuclein immunoreactivity at the synapse and their relationship with synapse size. Main analyses were performed in blocks from cingulate cortex and confirmed in blocks from the striatum of cases with dementia with Lewy bodies. A total of 1 318 700 single pre- or postsynaptic terminals were analysed. We found that phosphorylated α-synuclein is present exclusively in dementia with Lewy bodies cases, where it can be identified in the form of Lewy bodies, Lewy neurites and small aggregates ($<0.16\,\mu m^3$). Between 19% and 25% of phosphorylated α-synuclein deposits were found in presynaptic terminals mainly in the form of small aggregates. Synaptic terminals that co-localized with small aggregates of phosphorylated α-synuclein were significantly larger than those that did not. Finally, a gradient of phosphorylated α-synuclein aggregation in synapses (pre > pre + post > postsynaptic) was observed. These results indicate that phosphorylated α-synuclein is found at the presynaptic terminals of dementia with Lewy bodies cases mainly in the form of small phosphorylated α-synuclein aggregates that are associated with changes in synaptic morphology. Overall, our data support the notion that pathological phosphorylated α-synuclein may disrupt the structure and function of the synapse in dementia with Lewy bodies.

1 Memory Unit, Department of Neurology, Institut d'Investigacions Biomèdiques Sant Pau - Hospital de Sant Pau, Universitat Autònoma de Barcelona, Barcelona, Spain
2 Centro de Investigación Biomédica en Red en Enfermedades Neurodegenerativas (CIBERNED), Madrid, Spain
3 The University of Edinburgh, UK Dementia Research Institute, Centre for Discovery Brain Sciences, Edinburgh Neuroscience, Euan MacDonald Centre, and Centre for Dementia Prevention, Edinburgh, EH8 9JZ, UK
4 University of Edinburgh, Centre for Clinical Brain Sciences, Edinburgh, UK
5 Massachusetts General Hospital and Harvard Medical School, Charlestown, MA, USA
6 ICFO-Institut de Ciències Fotòniques, The Barcelona Institute of Science and Technology, Castelldefels, Barcelona, Spain
7 Neurological Tissue Bank of the Biobanc-Hospital Clinic-IDIBAPS, Barcelona Spain

Received May 9, 2017. Revised August 2, 2017. Accepted August 24, 2017.

Correspondence to: Dr Alberto Lleó
Department of Neurology, Hospital de la Santa Creu i Sant Pau
Sant Antoni Maria Claret, 167
08025 Barcelona, Spain
E-mail: alleo@santpau.es

Keywords: p-α-synuclein; dementia with Lewy bodies; synapses; array tomography; human tissue

Abbreviations: DLB = dementia with Lewy bodies; p-α-synuclein = α-synuclein phosphorylated at Ser129; PSD-95 = postsynaptic density protein 95; STED = stimulated emission depletion

Introduction

Dementia with Lewy bodies (DLB) is the second most common neurodegenerative dementia after Alzheimer's disease. The neuropathological hallmark of DLB is the formation of spherical inclusions in the neuronal somata called Lewy bodies and of elongated structures in dendritic or axonal compartments called Lewy neurites in the central and peripheral nervous systems (Goedert *et al.*, 2013).

In DLB, Lewy bodies and Lewy neurites are mainly composed of filaments of misfolded α-synuclein protein (Walker *et al.*, 2015). α-Synuclein is a synaptic protein that is located in presynaptic terminals where it contributes to neurotransmission and synaptic homeostasis (Maroteaux *et al.*, 1988; Iwai *et al.*, 1995; Clayton and George, 1999; Lashuel *et al.*, 2013; Burré, 2015; Calo *et al.*, 2016). Under pathological conditions α-synuclein is phosphorylated at residue Ser129 (p-α-synuclein). This phenomenon occurs constitutively at very low levels, but is markedly enhanced during pathological processes in which p-α-synuclein is detected in >90% of α-synuclein aggregates (Fujiwara *et al.*, 2002; Hasegawa *et al.*, 2002; Saito *et al.*, 2003; Anderson *et al.*, 2006; Muntané *et al.*, 2012). Growing evidence indicates that aggregation of α-synuclein at synapses is a major event in the pathogenesis of DLB and other α-synucleinopathies (Calo *et al.*, 2016). In particular, data from transgenic animal models suggest a toxic role of α-synuclein in synapses (Garcia-Reitböck *et al.*, 2010; Nemani *et al.*, 2010; Lundblad *et al.*, 2012; Calo *et al.*, 2016). In post-mortem brains from patients with DLB, p-α-synuclein is detected in synaptic-enriched fractions (Muntané *et al.*, 2008; Walker *et al.*, 2013) and α-synuclein forms small proteinase K-resistant aggregates in presynaptic terminals (Kramer and Schulz-Schaeffer, 2007; Tanji *et al.*, 2010). These data suggest that, although Lewy bodies and Lewy neurites are the classical hallmarks of DLB and other α-synucleinopathies, accumulation of pathological α-synuclein at the synapse may be the main effector of the disease leading to synaptic dysfunction and loss. Nonetheless, the study of α-synuclein-mediated synaptic pathology in humans has remained elusive, in part because synapses are small structures difficult to resolve microscopically in human brain.

In the present work we applied array tomography, a technique based on the production of 70 nm consecutive sections combined with immunofluorescence, to image synaptic pathology in DLB under the diffraction limit of light (Micheva and Smith, 2007; Kay *et al.*, 2013). Array tomography requires special fixation conditions, which limits the samples available for this type of study. This technique has been applied previously to successfully demonstrate synaptic abnormalities in animal models of Alzheimer's disease and in human Alzheimer's disease brains (Koffie *et al.*, 2009, 2012; Jackson *et al.*, 2016). To our knowledge, this study is the first to use array tomography to quantitatively assess synaptic p-α-synuclein in DLB, which allowed us to resolve α-synuclein pathology in synaptic terminals in human brain samples.

Materials and methods

Standard protocol approvals and patient consent

All brain donors and/or next of kin had given written informed consent for the use of brain tissue for research. The study was approved by the local ethics committee of: the Hospital de Sant Pau, Barcelona, Spain; the Edinburgh Brain Bank ethics committee and the ACCORD medical research ethics committee (approval numbers LR/11/ES/0022, 16/ES/0084, and 15-HV-016; ACCORD is the Academic and Clinical Central Office for Research and Development, a joint office of the University of Edinburgh and NHS Lothian); and the Massachusetts Alzheimer's Disease Research Centre and Massachusetts General Hospital Neuropathology department with local Institutional Review Board regulations.

Subjects

Human brain samples were obtained from the Edinburgh Brain Bank (see Supplementary Table 1 for Medical Research Council codes), the Massachusetts Alzheimer's Disease Research Centre and the Neurological Tissue Bank (NTB) of the Biobanc-Hospital Clinic-IDIBAPS in Barcelona.

Brain sampling and processing protocols for neuropathological diagnoses were carried out following international recommendations as previously described (Colom-Cadena *et al.*, 2013; Kay *et al.*, 2013; Samarasekera *et al.*, 2013).

Patients fulfilling clinical and neuropathological criteria for DLB ($n = 5$) (McKeith *et al.*, 2005), Alzheimer's disease ($n = 5$) (Montine *et al.*, 2012), or healthy control cases ($n = 5$) were included in this study. Clinical and neuropathological data

were retrospectively obtained from the clinical charts available at the Edinburgh Brain Bank, the Massachusetts Alzheimer's Disease Research Centre and the NTB. Neuropathological stages were applied according to international recommendations for DLB (McKeith *et al.*, 2005) and Lewy body pathology (Braak *et al.*, 2003). In cases with concomitant Alzheimer's disease pathology, current National Institute of Ageing/Alzheimer Association guidelines were applied (Montine *et al.*, 2012).

Tissue processing for array tomography

Fresh brain tissue from all cases was processed immediately upon collection for array tomography as previously described (Micheva and Smith, 2007; Kay *et al.*, 2013). The processing was the same for all cases regardless of the collection centre. Briefly, 1 mm × 1 mm × 3 mm tissue blocks from the cingulate cortex comprising all cortical layers and the striatum (nucleus putamen) were sectioned. Tissue blocks were fixed in 4% paraformaldehyde and 2.5% sucrose in 20 mM phosphate-buffered saline pH 7.4 for up to 3 h. Samples were dehydrated through ascending concentrations of ethanol, embedded into LR white acrylic resin (Electron Microscopy Sciences) and introduced into gelatine capsules where resin was allowed to polymerize overnight at >50°C. After polymerization, tissue blocks were stored at room temperature until used.

70 nm-array production

LR white embedded tissue blocks were cut at 70 nm sections using an ultramicrotome (Leica) equipped with an Ultra Jumbo Diamond Knife 35° (Diatome). Ribbons of at least 30 consecutive sections were produced and collected in gelatine subbed coverslips. For each case, two adjacent blocks of the cingulate cortex and the putamen were processed as described below (see Fig. 1 for study design).

Immunofluorescence

Coverslips with 70 nm consecutive sections were stained as previously described (Kay *et al.*, 2013). Sections were incubated with Tris-glycine solution 5 min at room temperature followed by a blocking of unspecific antigens with a cold water fish blocking buffer (Sigma-Aldrich) for 30 min. Sections were then incubated for 2 h with the following primary antibodies: mouse anti-α-synuclein phosphorylated at serine 129 (dilution 1:50, clone P-α-synuclein #64, Wako), goat anti-synaptophysin (dilution 1:50, AF5555, R&D Systems) and rabbit anti-postsynaptic density protein 95 (PSD-95) (dilution 1:50, clone D27E11, Cell Signaling), rabbit anti-synapsin I (dilution 1:50, AB1543P, Millipore) or rabbit anti-α-synuclein (dilution 1:50, AB5038, Millipore). After Tris-buffered saline (TBS) washings, secondary fluorescent antibodies Alexa Fluor® 488, Alexa Fluor® 555 and Alexa Fluor® 647 (dilution 1:50, Invitrogen) were applied for 30 min. Sections were washed with TBS and samples were stained with Hoechst 33258 (dilution 1:100, Life Technologies) for 5 min for nuclei visualization. Finally, coverslips were mounted on microscope slides with Immu-Mount (Fisher Scientific) mounting media.

Image acquisition

Images of the same region were acquired in consecutive sections using an Olympus BX61 microscope equipped with: 454, 488, 555 and 647 single-band pass filters (49000, 49002, 49004 and 49009, respectively, Chroma); an Orca Flash 4.0 LT camera (Hamamatsu); and a 64 × 1.2 NA Plan Apochromat objective (Olympus) controlled with HCImage software (Hamamatsu). For stimulated emission depletion (STED) microscopy, images from one representative DLB case were acquired using a TCS 5 STED CW microscope (Leica Microsystems). The CW STED laser operates at the wavelength of 592 nm and imaging is performed using hybrid detectors. The system performance has been fully characterized and a complete analysis of the achieved transversal resolution can be found elsewhere (Merino *et al.*, 2017). Sections with omission of antibodies or with secondary antibodies only were imaged to ensure specific and independent fluorophore visualization. For co-localization purposes, images were acquired avoiding saturated pixels. Saturation was only minimally applied for figure visualization. For each case, three fields of each section were imaged comprising all cortical layers (Fig. 1).

Image processing and analysis

Image stacks of each channel comprising all 70 nm consecutive sections were first registered as previously described (Kay *et al.*, 2013) using Multistackreg 1.4 ImageJ plugin [courtesy of Brad Busse based on Thévenaz *et al.* (1998)], based on a rigid registration followed by an affine registration of a reference channel that is applied to the other channels.

After alignment, identification of immunofluorescent objects and quantification of overlapping objects was achieved using an in-house semi-automatic algorithm (Fig. 1). Aligned sections were segmented using an automated local thresholding. Additionally, objects that were not in at least two consecutive sections were considered background and removed. Segmentation parameters were exclusive for each channel, but were the same for all included cases. A total of 1 318 700 single pre- or postsynaptic terminals were identified.

After identification of 3D objects, three different analyses were performed: (i) the density of objects for each channel subtracting the area occupied by cell bodies and/or blood vessels using a mask of the maximum intensity projection of the synaptophysin channel; (ii) the proportion of channel objects that overlap with objects from another channel; and (iii) the median size of all objects and of those co-localizing (Fig. 1). The in-house semi-automatic algorithm can be freely accessed at https://github.com/MemoryUnitSantPau.

Experimental design

The immunostaining, image acquisition, and image processing and analyses were carried out blinded to the clinicopathological diagnosis by assigning a random code to each sample.

Statistical analysis

Kruskal-Wallis with uncorrected Dunn's analysis *post hoc* tests were used to compare differences between three groups in p-α-synuclein densities, co-localization percentages or object sizes.

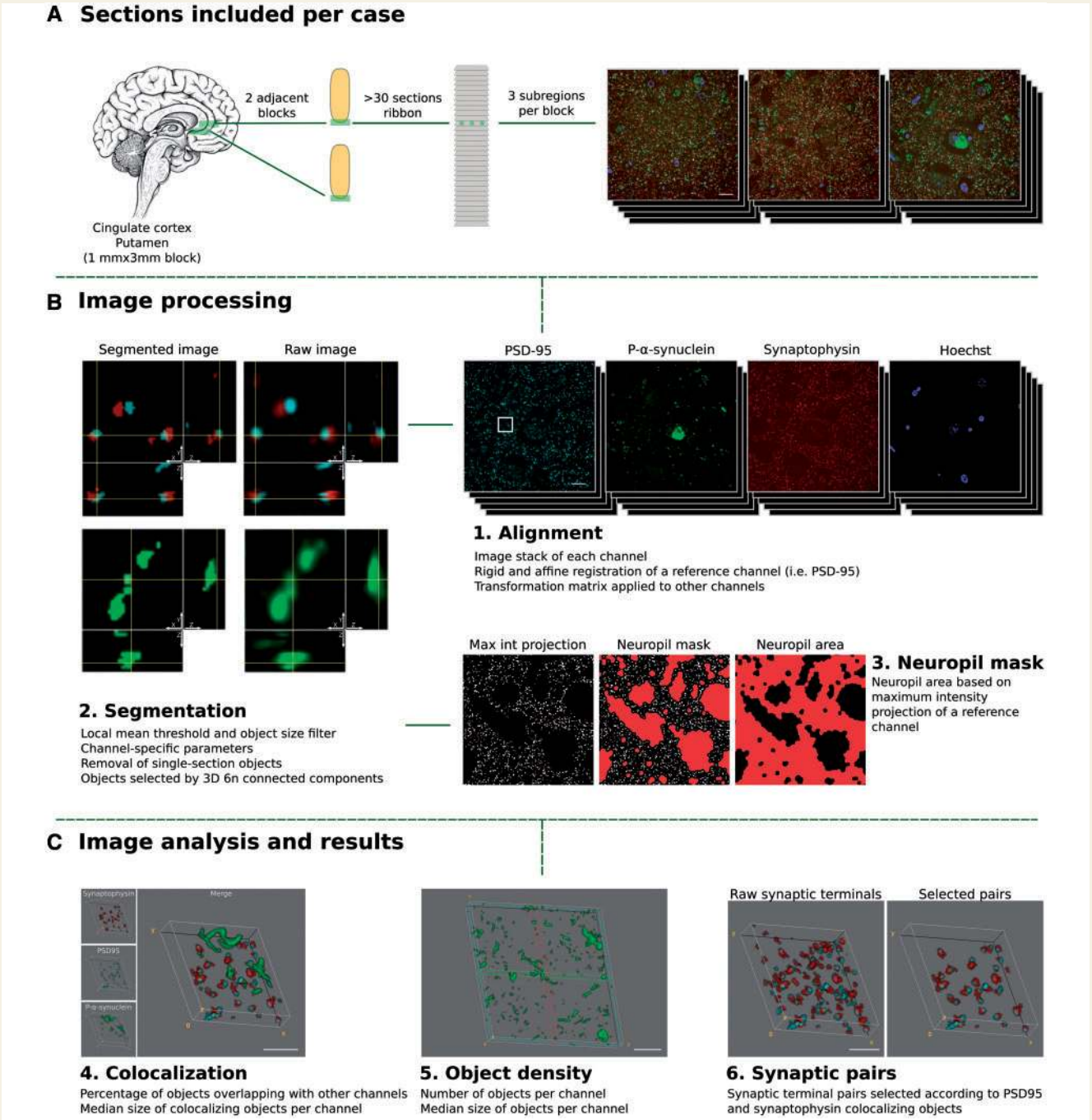

Figure 1 Study design. Tissue collection and processing of each case is shown in **A**. For each case, two adjacent tissue sections of cingulate cortex or the striatum (putamen nucleus) were processed and embedded in LR white. For each block a ribbon of >40 consecutive sections of 70 nm was produced. Each ribbon was immunostained for synaptophysin (red), p-α-synuclein (green) and PSD-95 (cyan), synapsin I or α-synuclein, and nuclei were visualized with Hoechst 33258 (blue). Three subregions were imaged through the entire ribbon. (**B** and **C**) Processing and analysis of the images. 1. First, individual channel stacks were produced, with all consecutive sections imaged. Consecutive sections of a reference channel (i.e. synaptophysin) were registered using a rigid and an affine transformation. Transformation matrices were applied to other channels. 2. Second, images were segmented using an in-house algorithm based on local mean threshold segmentation, removing single section objects, filtering by size, and detecting 3D objects as six neighbour connected components. Raw images (*right*) and segmented (*left*) representative images are shown. Each image corresponds to a single 70 nm section with its corresponding orthogonal views. 3. Neuropil area was calculated based on a maximum intensity projection of synaptophysin channel. 4. Co-localization between the channels of interest and the sizes of co-localizing objects was calculated. 5. The object density and object size were quantified and (6) for entire synaptic studies, segmented images of synaptophysin (pre-synaptic) and PSD-95 (postsynaptic) channels combined to remove all those objects without pre- and postsynaptic pairs. Max Int = maximum intensity; 6 n = six neighbour. Scale bars in **A** and **B** = 10 μm; **C** = 2 μm.

Statistical significance was set at 5% ($\alpha = 0.05$). All data were analysed using the Statistical Package for the Social Sciences version 19.0 (SPSS Inc., Chicago, IL, USA).

Results

Demographic, clinical and neuropathological characteristics of cases

Demographic, clinical and neuropathologic data are shown in Table 1. As expected, the DLB group exhibited advanced α-synuclein pathology as assessed by McKeith types and Lewy body Braak stages. A group of healthy subjects and Alzheimer's disease cases were included as controls for the array tomography analyses.

Phosphorylated α-synuclein is located in DLB presynaptic terminals

P-α-synuclein immunoreactivity in DLB was detected in array tomography in the form of Lewy bodies, Lewy neurites as well as small aggregates, the latter being defined as objects $<0.16\,\mu m^3$ without a clear dendritic or axonal morphology (Fig. 2A and B). Occasionally, p-α-synuclein immunoreactivity in cell nuclei was also observed. Quantification of total p-α-synuclein aggregates confirmed that pathology was restricted to DLB in array tomography, with negligible levels in Alzheimer's disease and controls (Fig. 2C). In contrast, immunofluorescence for non-phosphorylated α-synuclein showed a diffuse punctate pattern in grey matter in both controls and DLB. There was a high degree of overlap between p-α-synuclein and non-phosphorylated α-synuclein in DLB aggregates (Supplementary Fig. 1). Therefore, we chose p-α-synuclein as a marker to investigate the synaptic pathology in DLB.

We found that 19.17 ± 4.4% of p-α-synuclein aggregates co-localized with synaptophysin-positive terminals in the cingulate cortex (Fig. 2D, Supplementary Fig. 2 and Supplementary Video 1). These data were consistent across cases and revealed that most of the p-α-synuclein present at the pre-synapse consisted of small aggregates (76.6 ± 4%), while medium-sized aggregates or Lewy neurites were less abundant (23.4 ± 4%). As expected, no co-localization was found between Lewy bodies and synaptic terminals. Of the total synaptophysin-positive synaptic terminals analysed in DLB cases ($n = 252\ 696$), 2.7 ± 1% contained p-α-synuclein.

The presynaptic localization of p-α-synuclein aggregates was confirmed using synapsin I as an additional presynaptic marker. We found that 25.9 ± 7.3% of p-α-synuclein aggregates co-localized with synapsin I-positive terminals (Supplementary Fig. 3). As expected, most synapsin I-positive terminals co-localized with synaptophysin.

We used the striatum (putamen) as an additional region to confirm these findings. We found that 19.68 ± 12.7% of p-α-synuclein aggregates in the putamen were co-localizing with synaptophysin-positive presynaptic terminals.

Presynaptic terminal size and phosphorylated α-synuclein aggregation

Synaptic terminals that co-localized with small aggregates of p-α-synuclein were 1.43 ± 0.17-fold larger than those that did not ($P = 0.014$, Fig. 3). Interestingly, this difference was not observed when comparing the size of synaptophysin terminals without p-α-synuclein with those that co-localized with Lewy neurites.

Table 1 Demographic, clinical and neuropathologic data of control, DLB and Alzheimer's disease cases

Case	Diagnosis	Gender	Age at death	PMI, h	McKeith type	LB Braak stage	Braak NFT stage
1	Control	M	82	24	-	0	0
2	Control	M	63	16	-	0	0
3	Control	F	77	75	-	0	I
4	Control	M	78	39	-	0	I
5	Control	F	83	8	-	0	II
6	DLB	M	71	8	Neocortical	5	III
7	DLB	M	83	24	Neocortical	5	IV
8	DLB	F	62	9	Neocortical	5	IV
9	DLB	M	77	36	Neocortical	5	III
10	DLB	F	83	24	Neocortical	6	VI
11	AD	M	81	74	-	0	V
12	AD	M	72	109	-	0	VI
13	AD	M	81	83	-	0	VI
14	AD	M	85	91	-	0	VI
15	AD	F	90	18	-	0	V

AD = Alzheimer's disease; LB = Lewy body; NFT = neurofibrillary tangle; PMI = post-mortem interval.

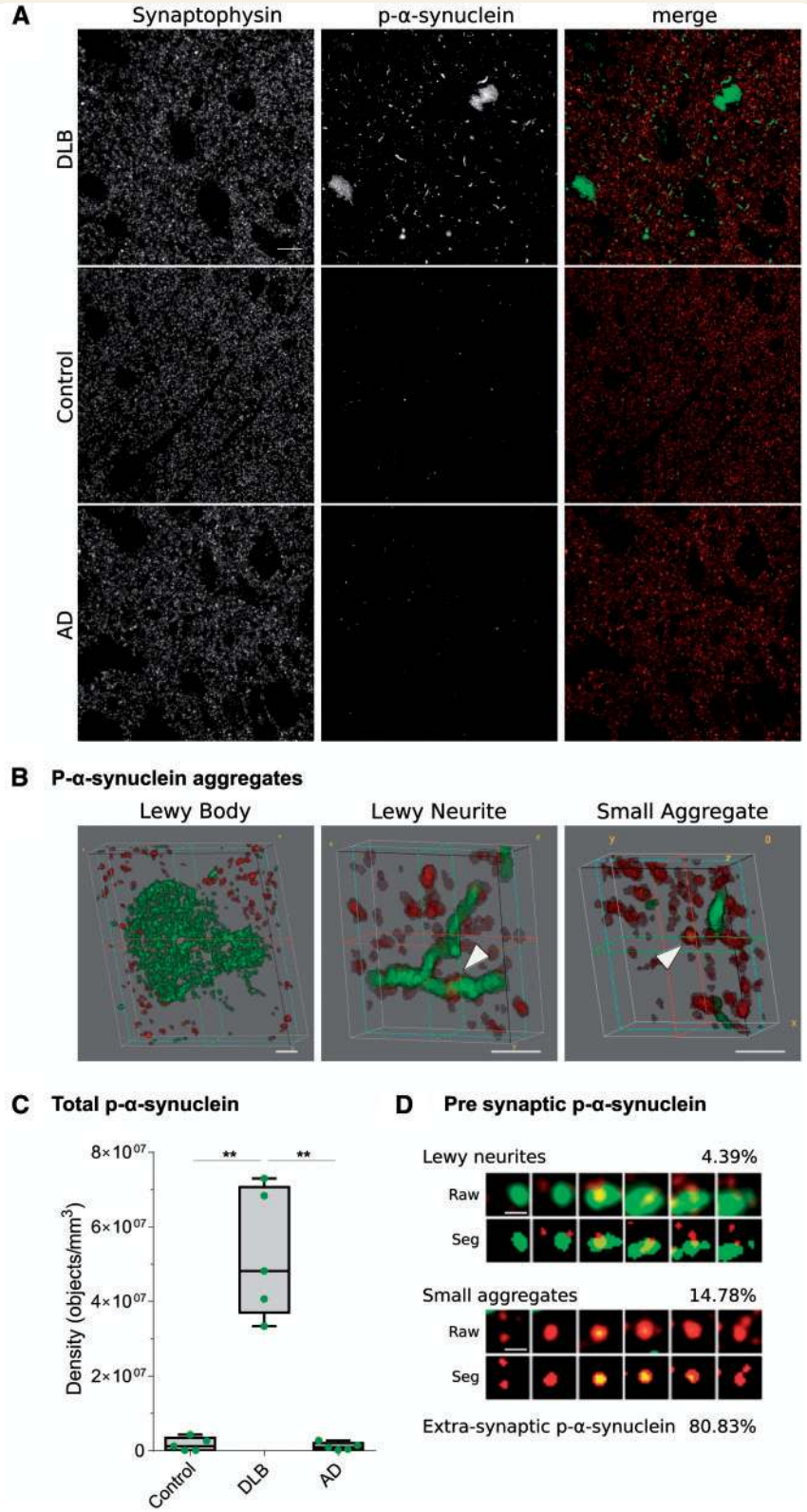

Figure 2 P-α-synuclein immunoreactivity patterns and synaptic localization. (**A**) Representative images of DLB, control and Alzheimer's disease cases stained with antibodies against synaptophysin (red) and p-α-synuclein (green). Each image is a maximum intensity projection of 31 consecutive sections. (**B**) Representative 3D representations of types of p-α-synuclein aggregates (green) found in DLB cases and synaptophysin terminals (red). Lewy bodies did not co-localize with synaptophysin terminals, while Lewy neurites and small aggregates did (arrowheads). (**C**) The quantification of total p-α-synuclein objects revealed that pathology was found almost exclusively in DLB cases (**$P < 0.01$). (**D**) Synaptograms representing six 70 nm consecutive sections (from *left* to *right*) of the Lewy neurite (LN) or small aggregate (SA) indicated by the arrowheads in **B**. Both the raw and segmented images are shown. The percentages of presynaptic p-α-synuclein found of Lewy neurites or small aggregate and extra-synaptic p-α-synuclein are indicated. AD = Alzheimer disease. Scale bar in **A** = 10 μm; **B** = 2 μm; **D** = 1 μm.

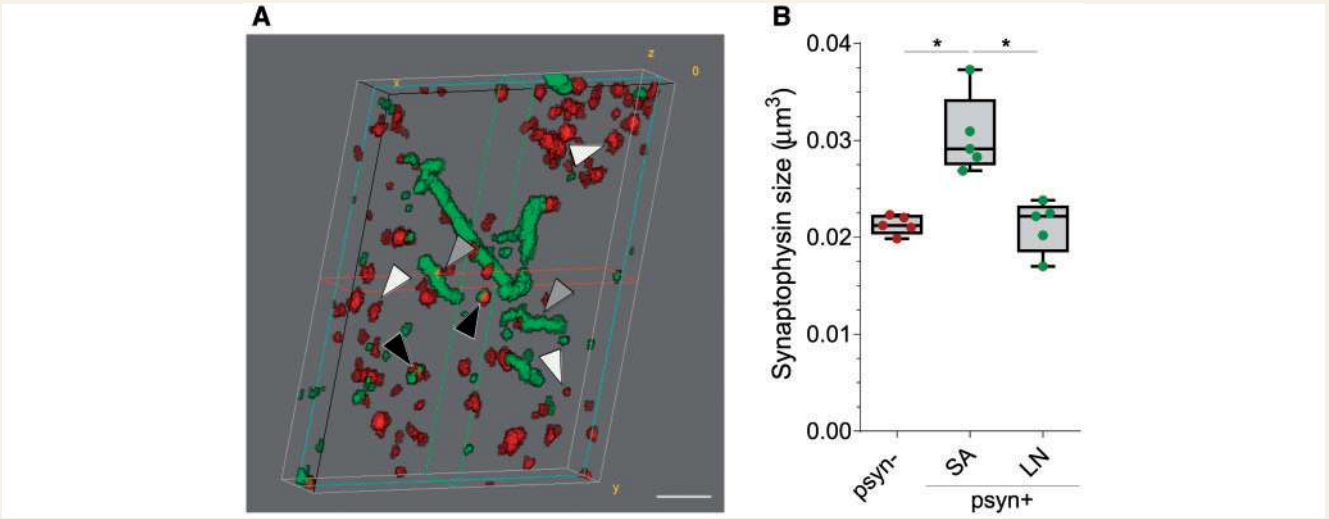

Figure 3 Median volume of presynaptic terminals co-localizing with p-α-synuclein. (**A**) 3D reconstruction of 20 consecutive sections from a DLB case. P-α-synuclein (green) and synaptophysin (red) are shown. Black arrowheads indicate synaptophysin objects that co-localize with small aggregates of p-α-synuclein, grey arrowheads point to synaptic terminals that co-localize with Lewy neurites, and white arrowheads those synaptophysin objects that do not co-localize with p-α-synuclein. (**B**) Median volumes of synaptic terminals according to co-localization with p-α-synuclein (p-α-synuclein +, or −) and their characteristic pattern (small aggregate or Lewy neurite, $*P < 0.05$). LN = Lewy neurite; Psyn = p-α-synuclein; SA = small aggregate. Scale bar in **A** = 2 μm.

Trans-synaptic localization of phosphorylated α-synuclein

Trans-synaptic propagation of p-α-synuclein pathology has been proposed as a common mechanism in synucleinopathies (Recasens and Dehay, 2014). To investigate this phenomenon *in vivo*, we next selected those synaptophysin presynaptic terminals that were opposed to objects labelled with the postsynaptic terminal marker PSD-95 (Fig. 4A). In those paired terminals, we observed that p-α-synuclein was more frequently located in presynaptic terminals (49.82 ± 4.3%, Fig. 4B), followed by a both pre- and postsynaptic localization (33.99 ± 2.4%) and less frequently in the postsynaptic density only (16.18 ± 3%). The synaptic gradient of p-α-synuclein was also observed in the striatum, with a more pronounced presynaptic predominance (70.14 ± 11.2% presynaptic only, 23.13 ± 13.7% pre- and postsynaptic, 6.73 ± 5.2% postsynaptic only). The postsynaptic terminal localization of p-α-synuclein was also confirmed by using STED microscopy to increase the lateral resolution (Fig. 4C). These data confirm that although p-α-synuclein aggregates are preferentially located at the pre-synapse, they can be independently found at the post-synapse as well.

Discussion

In the present study we have shown by array tomography that aggregates of p-α-synuclein were present at the synapse in DLB cases. In presynaptic terminals, the majority of p-α-synuclein was found in the form of small aggregates, while other types of aggregates, like Lewy neurites, were less abundant. Moreover, these small aggregates were associated with structural changes in presynaptic terminals. Finally, we observed a gradient of p-α-synuclein aggregates from the pre- to postsynaptic compartments.

There is growing evidence that synaptic abnormalities in DLB precede neuronal loss and Lewy body formation (Chung *et al.*, 2009; Nikolaus *et al.*, 2009; Calo *et al.*, 2016; Henstridge *et al.*, 2016) and that these synaptic defects are closely related with clinical symptoms (Vallortigara *et al.*, 2014; Whitfield *et al.*, 2014; Bereczki *et al.*, 2016). However, the investigation of DLB as a primary synaptopathy has been hampered by our technical ability to study synapses in human brain. The small size of synaptic terminals falls under the diffraction limit of light, which limits the use of conventional optical microscopy techniques for this purpose. Electron microscopy, which has been the standard technique to resolve the structure of synapses, only permits the reconstruction of small brain volumes and is less amenable to labelling multiple proteins (O'Rourke *et al.*, 2012).

In the present work, we applied array tomography to image synaptic pathology in DLB under the diffraction limit of light (Micheva and Smith, 2007; Kay *et al.*, 2013). To our knowledge, this is the first study to apply array tomography in DLB brains, a technique that has allowed us to perform large-scale quantitative synaptic imaging. We analysed 1 318 700 single pre- or postsynaptic terminals together with p-α-synuclein with very high spatial resolution. Previous studies have investigated synaptic proteins in DLB brains using conventional immunohistochemistry (Wakabayashi *et al.*, 1994; Revuelta *et al.*, 2008; Scott

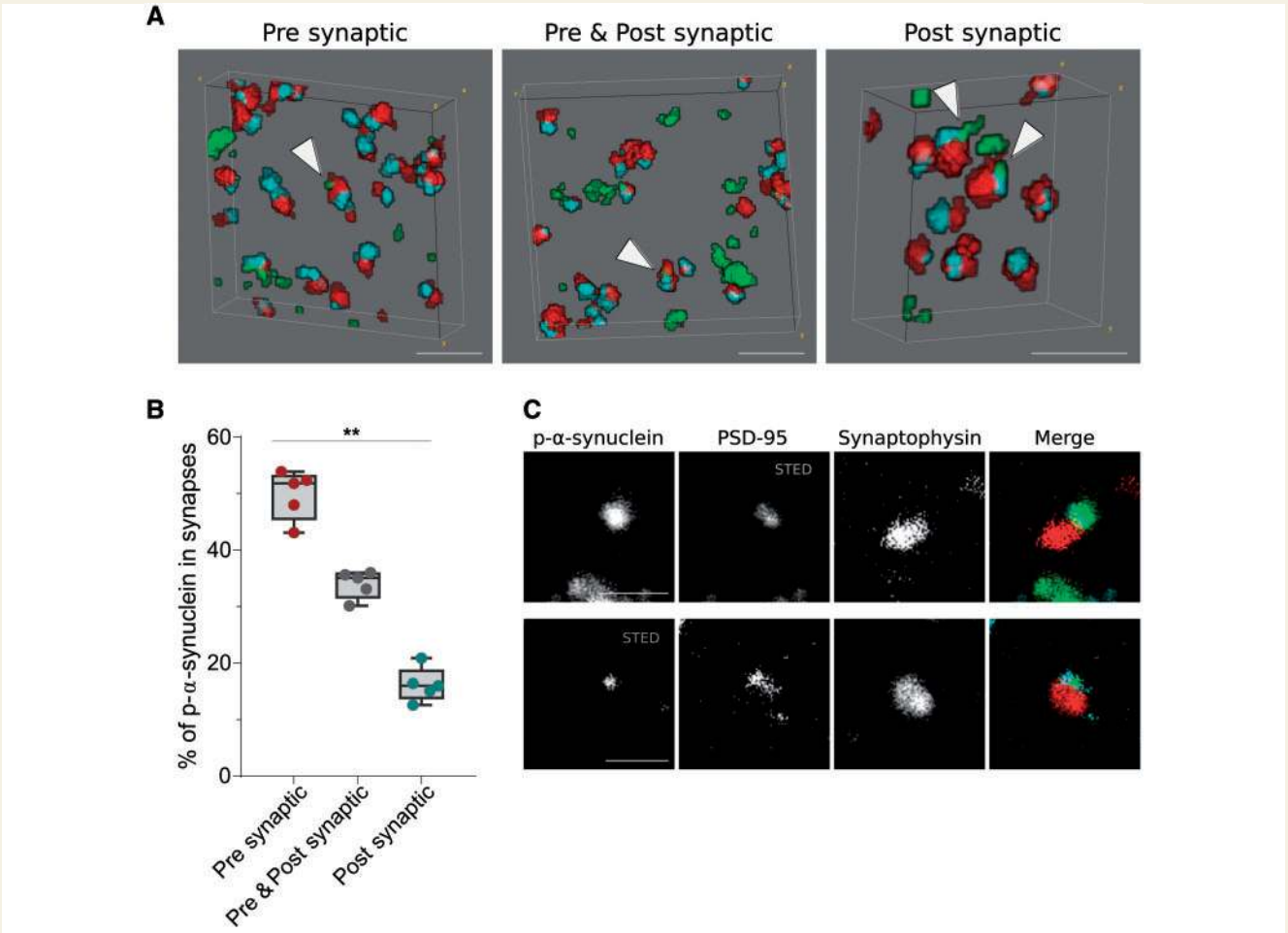

Figure 4 Trans-synaptic localization of p-α-synuclein. (**A**) 3D reconstruction of 20 consecutive sections from a DLB case. P-α-synuclein (green), synaptophysin (red) and PSD-95 (blue) are shown. White arrowheads point to zones where p-α-synuclein co-localizes with synaptophysin (presynaptic), PSD-95 (postsynaptic) or both (pre- and postsynaptic). In **B**, p-α-synuclein objects that co-localized with synaptic pairs (synaptophysin and PSD-95 objects) are classified depending on its presynaptic, pre- and postsynaptic or postsynaptic localization. The relative co-localization of p-α-synuclein with the synaptophysin presynaptic marker was significantly higher than the PSD-95 postsynaptic co-localization. (**C**) Representative images of the co-localization between between p-α-synuclein, synaptophysin and PSD-95 using array tomography combined with STED microscopy. A single 70 nm-thick section stained for p-α-synuclein (green), synaptophysin (red) and PSD-95 (blue) is shown. STED was applied to image PSD-95 (*top row*) or p-α-synuclein (*bottom row*). Scale bar in **A** = 2 μm; **C** = 1 μm.

et al., 2010) or biochemical analysis of brain homogenates (Masliah *et al.*, 1993; Brown *et al.*, 1998; Hansen *et al.*, 1998; Campbell *et al.*, 2000; Reid *et al.*, 2000; Kramer and Schulz-Schaeffer, 2007; Mukaetova-Ladinska *et al.*, 2013; Khundakar *et al.*, 2016; Xing *et al.*, 2016). In some of these studies, p-α-synuclein and proteinase K-resistant α-synuclein aggregates were found in synaptic-enriched fractions (Kramer and Schulz-Schaeffer, 2007; Muntané *et al.*, 2008; Tanji *et al.*, 2010; Walker *et al.*, 2013). However, many of these studies could not specifically address the precise synaptic localization due to the low resolution of the techniques used. Our results confirm and expand on these observations in intact brain samples by using a technique especially suited for the analysis of human brain synapses.

We found that ~20% of p-α-synuclein aggregates were co-localizing with synaptophysin-positive terminals in the cingulate cortex and striatum. The percentage was a slightly higher (25%) when using synapsin I as a presynaptic marker. The detection of p-α-synuclein at presynaptic compartments suggests a role in synaptic degeneration. Notably, we found that small α-synuclein aggregates are the most common form in synapses. A previous study (Kramer and Schulz-Schaeffer, 2007) described proteinase K-resistant aggregates in presynaptic compartments that represented the 50–90% of α-synuclein aggregates. We found a much lower percentage of α-synuclein aggregates at the presynaptic terminals. This difference may be due to numerous methodological differences: the antibodies used; the methods to detect synapses and pathological aggregates;

or our stringent protocol used to define p-α-synuclein and presynaptic objects. Despite these methodological issues, we found that 77% of p-α-synuclein aggregates in contact with presynaptic terminals are small aggregates. Taken together, both studies support the notion of small α-synuclein aggregates as key pathological forms in driving synaptic damage and dysfunction (Schulz-Schaeffer, 2010).

Our results are also in line with the hypothesis that the presynaptic terminal is an early site of α-synuclein aggregation in DLB and other α-synucleinopathies, the same site where it is found under physiological conditions (Lashuel *et al.*, 2013; Spinelli *et al.*, 2014; Volpicelli-Daley *et al.*, 2014; Majd *et al.*, 2015; Abeliovich and Gitler, 2016). The aggregation of α-synuclein may lead to abnormal functional impairment of neurotransmitter release (Garcia-Reitböck *et al.*, 2010; Nemani *et al.*, 2010), subsequent to axonal transport defects through the impairment of endosome and/or autophagosome transport (Volpicelli-Daley *et al.*, 2014), which may lead to neurodegeneration (Ferrer *et al.*, 2001; Desplats *et al.*, 2009; Decressac *et al.*, 2013).

We also observed larger presynaptic terminal volume in the presence of p-α-synuclein. Interestingly, an inverse correlation has been observed between synaptic density and the size of remaining synapses in Alzheimer's disease as measured by the length of the postsynaptic density (DeKosky and Scheff, 1990; Scheff *et al.*, 1990; Scheff and Price, 1993). This enlargement of remaining synapses has been interpreted as a compensatory response, rather than as selective loss of small synapses. Our data could suggest a similar compensatory mechanism in synapses containing pathological p-α-synuclein.

Several previous studies in cellular and animal models have shown that α-synuclein may propagate along neural circuits following a hierarchical pattern (Eisbach and Outeiro, 2013; Masuda-Suzukake *et al.*, 2013; Recasens and Dehay, 2014). The observation of a spatial gradient in p-α-synuclein aggregation in synapses (pre > pre + post > postsynaptic) could be interpreted as a sign of trans-synaptic spreading of α-synuclein pathology. However, using STED microscopy we found that although p-α-synuclein predominates at the pre-synapse it can also be found independently at the post-synapse. Due to the inherent descriptive nature of post-mortem studies and the difficulties to identify the synaptic cleft, additional research is needed to elucidate if our findings are related to α-synuclein spreading and/or independent aggregation in both synaptic compartments.

Despite the limitations of our study—relatively small sample size, inclusion of cases with advanced disease stages, or analysis of a single phospho-epitope of p-α-synuclein—our findings are important as they demonstrate for the first time that p-α-synuclein accumulates in presynaptic terminals by large-scale imaging of synapses in DLB brain. Taken together, the present work provides a visual and quantitative evidence of the synaptic deposition of small p-α-synuclein aggregates in presynaptic terminals. This study supports the hypothesis that DLB and other α-synucleinopathies are primary synaptopathies. These data should stimulate the search for therapies aimed at reducing synaptic α-synuclein-induced damage or spread.

Acknowledgements

The authors would like to thank all brain donors and their relatives for generous brain donation for research as well as the brain banks for tissue supply. This research has been supported by Fundació Cellex Barcelona.

Funding

This work was supported by FISPI14/1561, Fondo Europeo de Desarrollo Regional (FEDER), Unión Europea, "Una manera de hacer Europa", PERIS SLT002/16/00408-01 and Marató TV3 to Alberto Lleó and CIBERNED. C.S. and C-A.M. were funded by MRC grant MR/L016400/1. C.H. is funded by a project grant from MND Scotland. The Massachusetts Alzheimer Disease Research Center is supported by funding from the NIH (P50 AG005134). T.S-J. is funded by the European Research Council (Consolidator award ALZSYN), Alzheimer's Research UK, the Scottish Government Chief Scientists' Office, Alzheimer's Society, UK Dementia Research Institute and Wellcome Trust/University of Edinburgh Institutional Strategic Support Funding. P.L-A. is funded by The Spanish Ministry of Economy and Competitiveness, through the "Severo Ochoa" Programme for Centres of Excellence in R&D (SEV- 2015-0522) and the CERCA Programme/Generalitat de Catalunya.

Supplementary material

Supplementary material is available at *Brain* online.

References

Abeliovich A, Gitler AD. Defects in trafficking bridge Parkinson's disease pathology and genetics. Nature 2016; 539: 207–16.

Anderson JP, Walker DE, Goldstein JM, De Laat R, Banducci K, Caccavello RJ, et al. Phosphorylation of Ser-129 is the dominant pathological modification of α-synuclein in familial and sporadic lewy body disease. J Biol Chem 2006; 281: 29739–52.

Bereczki E, Francis PT, Howlett D, Pereira JB, Höglund K, Bogstedt A, et al. Synaptic proteins predict cognitive decline in Alzheimer's disease and Lewy body dementia. Alzheimers Dement 2016; 12: 1149–58.

Braak H, Del Tredici K, Rüb U, De Vos RAI, Jansen Steur ENH, Braak E. Staging of brain pathology related to sporadic Parkinson's disease. Neurobiol Aging 2003; 24: 197–211.

Brown DF, Risser RC, Bigio EH, Tripp P, Stiegler A, Welch E, et al. Neocortical synapse density and Braak stage in the Lewy body variant of Alzheimer disease: a comparison with classic Alzheimer disease and normal aging. J Neuropathol Exp Neurol 1998; 57: 955–60.

Burré J. The synaptic function of alpha-synuclein. J Parkinsons Dis 2015; 5: 699–713.
Calo L, Wegrzynowicz M, Santivañez-Perez J, Grazia Spillantini M. Synaptic failure and α-synuclein. Mov Disord 2016; 31: 169–77.
Campbell BC, Li QX, Culvenor JG, Jäkälä P, Cappai R, Beyreuther K, et al. Accumulation of insoluble alpha-synuclein in dementia with Lewy bodies. Neurobiol Dis 2000; 7: 192–200.
Chung CY, Koprich JB, Siddiqi H, Isacson O. Dynamic changes in presynaptic and axonal transport proteins combined with striatal neuroinflammation precede dopaminergic neuronal loss in a rat model of AAV alpha-synucleinopathy. J. Neurosci. 2009; 29: 3365–73.
Clayton DF, George JM. Synucleins in synaptic plasticity and neurodegenerative disorders. J Neurosci Res 1999; 58: 120–9.
Colom-Cadena M, Gelpi E, Charif S, Belbin O, Blesa R, Marti MJ, et al. Confluence of alpha-synuclein, tau, and beta-amyloid pathologies in dementia with Lewy bodies. J Neuropathol Exp Neurol 2013; 72: 1203–12.
Decressac M, Mattsson B, Weikop P, Lundblad M, Jakobsson J, Björklund A. TFEB-mediated autophagy rescues midbrain dopamine neurons from α-synuclein toxicity. Proc Natl Acad Sci USA 2013; 110: E1817–26.
DeKosky ST, Scheff SW. Synapse loss in frontal cortex biopsies in Alzheimer's disease: correlation with cognitive severity. Ann Neurol 1990; 27: 457–64.
Desplats P, Lee H-J, Bae E-J, Patrick C, Rockenstein E, Crews L, et al. Inclusion formation and neuronal cell death through neuron-to-neuron transmission of alpha-synuclein. Proc Natl Acad Sci USA 2009; 106: 13010–15.
Eisbach SE, Outeiro TF. Alpha-Synuclein and intracellular trafficking: impact on the spreading of Parkinson's disease pathology. J Mol Med 2013; 91: 693–703.
Ferrer I, Blanco R, Carmona M, Puig B, Barrachina M, Gómez C, et al. Active, phosphorylation-dependent mitogen-activated protein kinase (MAPK/ERK), stress-activated protein kinase/c-Jun N-terminal kinase (SAPK/JNK), and p38 kinase expression in Parkinson's disease and Dementia with Lewy bodies. J Neural Transm 2001; 108: 1383–96.
Fujiwara H, Hasegawa M, Dohmae N, Kawashima A, Masliah E, Goldberg MS, et al. α-Synuclein is phosphorylated in synucleinopathy lesions. Nat Cell Biol 2002; 4: 160–4.
Garcia-Reitböck P, Anichtchik O, Bellucci A, Iovino M, Ballini C, Fineberg E, et al. SNARE protein redistribution and synaptic failure in a transgenic mouse model of Parkinson's disease. Brain 2010; 133: 2032–44.
Goedert M, Spillantini MG, Del Tredici K, Braak H. 100 years of Lewy pathology. Nat Rev Neurol 2013; 9: 13–24.
Hansen LA, Daniel SE, Wilcock GK, Love S. Frontal cortical synaptophysin in Lewy body diseases: relation to Alzheimer's disease and dementia. J Neurol Neurosurg Psychiatry 1998; 64: 653–6.
Hasegawa M, Fujiwara H, Nonaka T, Wakabayashi K, Takahashi H, Lee VMY, et al. Phosphorylated alpha-synuclein is ubiquitinated in alpha-synucleinopathy lesions. J Biol Chem 2002; 277: 49071–6.
Henstridge CM, Pickett E, Spires-Jones TL. Synaptic pathology: a shared mechanism in neurological disease. Ageing Res Rev 2016; 28: 72–84.
Iwai A, Masliah E, Yoshimoto M, Ge N, Flanagan L, Rohan de Silva HA, et al. The precursor protein of non-Abeta component of Alzheimer's disease amyloid is a presynaptic protein of the central nervous system. Neuron 1995; 14: 467–75.
Jackson RJ, Rudinskiy N, Herrmann AG, Croft S, Kim JM, Petrova V, et al. Human tau increases amyloid β plaque size but not amyloid β-mediated synapse loss in a novel mouse model of Alzheimer's disease. Eur J Neurosci 2016; 44: 3056–66.
Kay KR, Smith C, Wright AK, Serrano-Pozo A, Pooler AM, Koffie R, et al. Studying synapses in human brain with array tomography and electron microscopy. Nat Protoc 2013; 8: 1366–80.
Khundakar AA, Hanson PS, Erskine D, Lax NZ, Roscamp J, Karyka E, et al. Analysis of primary visual cortex in dementia with Lewy bodies indicates GABAergic involvement associated with recurrent complex visual hallucinations. Acta Neuropathol Commun 2016; 4: 66.
Koffie RM, Hashimoto T, Tai HC, Kay KR, Serrano-Pozo A, Joyner D, et al. Apolipoprotein E4 effects in Alzheimer's disease are mediated by synaptotoxic oligomeric amyloid-beta. Brain 2012; 135: 2155–68.
Koffie RM, Meyer-Luehmann M, Hashimoto T, Adams KW, Mielke ML, Garcia-Alloza M, et al. Oligomeric amyloid beta associates with postsynaptic densities and correlates with excitatory synapse loss near senile plaques. Proc Natl Acad Sci USA 2009; 106: 4012–7.
Kramer ML, Schulz-Schaeffer WJ. Presynaptic alpha-synuclein aggregates, not Lewy bodies, cause neurodegeneration in dementia with Lewy bodies. J Neurosci 2007; 27: 1405–10.
Lashuel HA, Overk CR, Oueslati A, Masliah E. The many faces of α-synuclein: from structure and toxicity to therapeutic target. Nat Rev Neurosci 2013; 14: 38–48.
Lundblad M, Decressac M, Mattsson B, Björklund A. Impaired neurotransmission caused by overexpression of α-synuclein in nigral dopamine neurons. Proc Natl Acad Sci USA 2012; 109: 3213–19.
Majd S, Power JH, Grantham HJM. Neuronal response in Alzheimer's and Parkinson's disease: the effect of toxic proteins on intracellular pathways. BMC Neurosci 2015; 16: 69.
Maroteaux L, Campanelli JT, Scheller RH. Synuclein: a neuron-specific protein localized to the nucleus and presynaptic nerve terminal. J Neurosci 1988; 8: 2804–15.
Masliah E, Mallory M, DeTeresa R, Alford M, Hansen L. Differing patterns of aberrant neuronal sprouting in Alzheimer's disease with and without Lewy bodies. Brain Res 1993; 617: 258–66.
Masuda-Suzukake M, Nonaka T, Hosokawa M, Oikawa T, Arai T, Akiyama H, et al. Prion-like spreading of pathological alpha-synuclein in brain. Brain 2013; 136: 1128–38.
McKeith IG, Dickson DW, Lowe J, Emre M, O'Brien JT, Feldman H, et al. Diagnosis and management of dementia with Lewy bodies: third report of the DLB consortium. Neurology 2005; 65: 1863–72.
Merino D, Mallabiabarrena A, Andilla J, Artigas D, Zimmermann T, Loza-Alvarez P. STED imaging performance estimation by means of Fourier transform analysis. Biomed Opt Express 2017; 8: 2472–82.
Micheva KD, Smith SJ. Array tomography: a new tool for imaging the molecular architecture and ultrastructure of neural circuits. Neuron 2007; 55: 25–36.
Montine TJ, Phelps CH, Beach TG, Bigio EH, Cairns NJ, Dickson DW, et al. National institute on aging-Alzheimer's association guidelines for the neuropathologic assessment of Alzheimer's disease: a practical approach. Acta Neuropathol 2012; 123: 1–11.
Mukaetova-Ladinska EB, Andras A, Milne J, Abdel-All Z, Borr I, Jaros E, et al. Synaptic proteins and choline acetyltransferase loss in visual cortex in dementia with Lewy bodies. J Neuropathol Exp Neurol 2013; 72: 53–60.
Muntané G, Dalfó E, Martinez A, Ferrer I. Phosphorylation of tau and α-synuclein in synaptic-enriched fractions of the frontal cortex in Alzheimer's disease, and in Parkinson's disease and related α-synucleinopathies. Neuroscience 2008; 152: 913–23.
Muntané G, Ferrer I, Martinez-Vicente M. A-synuclein phosphorylation and truncation are normal events in the adult human brain. Neuroscience 2012; 200: 106–19.
Nemani VM, Lu W, Berge V, Nakamura K, Onoa B, Lee MK, et al. Increased expression of α-synuclein reduces neurotransmitter release by inhibiting synaptic vesicle reclustering after endocytosis. Neuron 2010; 65: 66–79.
Nikolaus S, Antke C, Müller HW. *In vivo* imaging of synaptic function in the central nervous system: II. Mental and affective disorders. Behav Brain Res 2009; 204: 32–66.
O'Rourke NA, Weiler NC, Micheva KD, Smith SJ. Deep molecular diversity of mammalian synapses: why it matters and how to measure it. Nat Rev Neurosci 2012; 13: 365–79.
Recasens A, Dehay B. Alpha-synuclein spreading in Parkinson's disease. Front Neuroanat 2014; 8: 159.

Reid RT, Sabbagh MN, CoreyBloom J, Tiraboschi P, Thal LJ. Nicotinic receptor losses in dementia with Lewy bodies: comparisons with Alzheimer's disease. Neurobiol Aging 2000; 21: 741–6.

Revuelta GJ, Rosso A, Lippa CF. Neuritic pathology as a correlate of synaptic loss in dementia with Lewy bodies. Am J Alzheimers Dis Other Demen 2008; 23: 97–102.

Saito Y, Kawashima A, Ruberu NN, Fujiwara H, Koyama S, Sawabe M, et al. Accumulation of phosphorylated a-synuclein in aging human brain. J Neuropathol Exp Neurol 2003; 62: 644–54.

Samarasekera N, Salman RAS, Huitinga I, Klioueva N, McLean CA, Kretzschmar H, et al. Brain banking for neurological disorders. Lancet Neurol. 2013; 12: 1096–105.

Scheff SW, DeKosky ST, Price DA. Quantitative assessment of cortical synaptic density in Alzheimer's disease. Neurobiol Aging 1990; 11: 29–37.

Scheff SW, Price DA. Synapse loss in the temporal lobe in Alzheimer's disease. Ann Neurol 1993; 33: 190–9.

Schulz-Schaeffer WJ. The synaptic pathology of α-synuclein aggregation in dementia with Lewy bodies, Parkinson's disease and Parkinson's disease dementia. Acta Neuropathol 2010; 120: 131–43.

Scott DA, Tabarean I, Tang Y, Cartier A, Masliah E, Roy S. A pathologic cascade leading to synaptic dysfunction in alpha-synuclein-induced neurodegeneration. Neurobiol Dis 2010; 30: 8083–95.

Spinelli KJ, Taylor JK, Osterberg VR, Churchill MJ, Pollock E, Moore C, et al. Presynaptic alpha-synuclein aggregation in a mouse model of Parkinson's disease. J Neurosci 2014; 34: 2037–50.

Tanji K, Mori F, Mimura J, Itoh K, Kakita A, Takahashi H, et al. Proteinase K-resistant alpha-synuclein is deposited in presynapses in human Lewy body disease and A53T alpha-synuclein transgenic mice. Acta Neuropathol 2010; 120: 145–54.

Thévenaz P, Ruttimann UE, Unser M. A pyramid approach to subpixel registration based on intensity. IEEE Trans Image Process 1998; 7: 27–41.

Vallortigara J, Rangarajan S, Whitfield D, Alghamdi A, Howlett D, Hortobágyi T, et al. Dynamin1 concentration in the prefrontal cortex is associated with cognitive impairment in Lewy body dementia. F1000Res 2014; 3: 108.

Volpicelli-Daley LA, Gamble KL, Schultheiss CE, Riddle DM, West AB, Lee VM-Y. Formation of α-synuclein Lewy neurite-like aggregates in axons impedes the transport of distinct endosomes. Mol Biol Cell 2014; 25: 4010–23.

Wakabayashi K, Honer WG, Masliah E. Synapse alterations in the hippocampal-entorhinal formation in Alzheimer's disease with and without Lewy body disease. Brain Res 1994; 667: 24–32.

Walker DG, Lue LF, Adler CH, Shill HA, Caviness JN, Sabbagh MN, et al. Changes in properties of serine 129 phosphorylated α-synuclein with progression of Lewy-type histopathology in human brains. Exp Neurol 2013; 240: 190–204.

Walker Z, Possin KL, Boeve BF, Aarsland D. Lewy body dementias. Lancet 2015; 386: 1683–97.

Whitfield DR, Vallortigara J, Alghamdi A, Howlett D, Hortobágyi T, Johnson M, et al. Assessment of ZnT3 and PSD95 protein levels in Lewy body dementias and Alzheimer's disease: association with cognitive impairment. Neurobiol Aging 2014; 35: 2836–44.

Xing H, Lim Y-A, Chong JR, Lee JH, Aarsland D, Ballard CG, et al. Increased phosphorylation of collapsin response mediator protein-2 at Thr514 correlates with β-amyloid burden and synaptic deficits in Lewy body dementias. Mol Brain 2016; 9: 84.